SAND2013-10639C

Experimental Investigation of Aspect-Ratio Effects in Transonic and Subsonic Rectangular Cavity Flow

Justin L. Wagner,[1] Steven J. Beresh,[2] Katya M. Casper,[3] Brian O. Pruett,[4] Russell W. Spillers,[5] and John F. Henfling[6]
Sandia National Laboratories, Albuquerque, NM, 87185

Experiments were conducted at freestream Mach numbers of 0.55, 0.80, and 0.90 in open cavities having a length to depth ratio *L/D* of 5. The boundary layer at the cavity entrance was turbulent with a thickness of about 0.5 *D*. The length to width ratio *L/W* was varied between 1.00, 1.67, and 5.00. Two stereoscopic PIV systems were used simultaneously to characterize the flow along the streamwise – wall normal symmetry plane. The recirculation region was weakest in the *L/W* = 1.67 flow, a trend previously observed at supersonic Mach numbers. The *L/W* = 1.00 cavity had the highest turbulence intensities and aft-wall pressure fluctuations. The two narrower cavities exhibited lower turbulence intensities and lower pressure fluctuations of a comparable level. The narrowest cavity exhibited the greatest spanwise coherence at the fore and aft walls; an observation possibly related to reduced spanwise flow in comparison to the wider cavities. Simultaneous pressure data showed the narrowest cavity to have modes two and three active for all Mach numbers. However, despite similar mean and turbulence fields, the *L/W* = 1.67 sound pressure level spectra varied significantly with Mach number.

I. Introduction

Flow over an open aircraft bay can produce intense structural vibrations, which are caused by high levels of aeroacoustic loading. This loading has a large broadband component owing to turbulent fluctuations. Additionally, under the right conditions, cavity resonant tones are produced [1]. These resonant tones can have very high sound pressure levels *SPL*, up to about 170 dB [2]. *SPLs* [3, 4] and resulting structural vibrations are known to scale with freestream dynamic pressure q_∞ [5]. The large levels of aeroacoustic loading in cavity flows has motivated many studies over the last sixty years, many of which are reviewed by Rockwell and Naudascher [6], Rowley and Williams [7], and Cattafesta et al. [8].

At Mach 5, there is evidence that cavity resonant tones can be reasonably predicted with closed-box acoustics theory [9]. For Mach numbers less than about 3[10], however, the dynamics of the cavity's separated shear layer become important to resonance. In subsonic and transonic flows, when the cavity length to depth ratio *L*/*D* is less than about 6-8 [3], and in supersonic flows when *L*/*D* is less than about 10 [9], the flow category is defined to be 'open.' In open cavity flow, the cavity's acoustic field and free shear layer interact to form a feedback loop that results in cavity resonance. The resonant modes are longitudinal and in simple rectangular geometries, their frequencies can be reasonably predicted by the semi-empirical relation of Rossiter [1], which was later modified by Heller and Bliss for supersonic Mach numbers [11]. Furthermore, the surface pressures in aircraft bay flows are highly complex functions of time and position. For instance, the dominant cavity mode can vary with time – a

[1] Senior Member of the Technical Staff, Engineering Sciences Center, P.O. Box 5800, Mailstop 0825; jwagner@sandia.gov. AIAA Member.
[2] Principal Member of the Technical Staff, Engineering Sciences Center, AIAA Associate Fellow.
[3] Senior Member of the Technical Staff, Engineering Sciences Center, AIAA Member.
[4] Senior Technologist, Engineering Sciences Center, AIAA Member.
[5] Principal Technologist, Engineering Sciences Center.
[6] Distinguished Technologist, Engineering Sciences Center.

This work is supported by Sandia National Laboratories and the United States Department of Energy. Sandia National Laboratories is a multi-program laboratory managed and operated by Sandia Corporation, a wholly owned subsidiary of Lockheed Martin Corporation, for the U.S. Department of Energy's National Nuclear Security Administration under contract DE-AC04-94AL85000

process known as mode-switching [12-14] – and surface pressures are known to be highly three-dimensional [15]. These spatial and temporal variations in pressure are then imparted onto a structure such as a store in an aircraft bay or landing gear in a wheel well.

Although the Rossiter relation [1, 11] is often effective in calculating the cavity resonant frequency values, the mode shapes, amplitudes, and energy distributions are less predictable as they are complex functions of flow conditions (Mach number, Reynolds number, boundary layer properties, etc.) and cavity geometry (L/D, length to width ratio L/W) [6-8, 16]. Several studies have measured the effects of aspect ratio L/W on cavity surface pressures [1, 3, 9]. Previous work has shown that narrower cavities transition to 'closed' (non-resonating) flows at lower L/D for subsonic [3] and supersonic [9] Mach number. Additionally, the aspect ratio has been observed to influence the overall sound pressure level *OASPL* [1, 3], as well as the spectra amplitudes [1, 3], although the physical mechanisms responsible for these width-dependent alterations remains unclear.

Recent work focused on fluid structure interactions (FSI) in compressible cavity flows has shown that the structural response to broadband pressure fluctuations can be quite high at structural natural frequencies. Moreover, structural vibration levels are particularly sensitive to cavity resonant tones in the streamwise and vertical directions [5]. Thus, ascertaining how and why geometrical parameters such as L/W influence both the *OASPL* and cavity mode amplitudes is critical to predicting loads imparted onto an internal structure. The understanding of such effects is, however, limited by a lack of quantitative flowfield data capturing the dynamics of the shear layer.

To remedy this, Beresh et al. [17] recently conducted particle image velocimetry (PIV) experiments in supersonic cavity flows over a Mach number range of 1.5 – 2.5 [17]. In the experiments, the cavity L/D was fixed at 5, and three different aspect ratios of 1.00, 1.67, and 5.00 were tested. The data showed both the mean flow and turbulence levels within the cavity to be a function of L/W. In particular at the middle L/W, compared to the other two aspect ratios the recirculation region was observed to be located farther upstream and the turbulence intensity in the streamwise – wall-normal symmetry plane was diminished. Moreover, data in the streamwise-spanwise plane suggested that lateral spillage at the cavity sidewalls played a critical role on mean flow structure and turbulence properties.

The current work extends the investigation of aspect ratio effects in compressible cavity flows to subsonic and transonic Mach numbers of 0.55, 0.80, and 0.90. PIV data provide mean and turbulence intensity fields, the trends of which are compared to the previous supersonic experiments [17]. Additionally, fast-response pressure measurements are presented to highlight the effects of cavity width on *OASPL*, flow three-dimensionality, and cavity modes.

II. Experimental Program

A. Trisonic Wind Tunnel (TWT)

Experiments were conducted in the blowdown-to-atmosphere TWT. The facility used air as the test gas and had a test section that was enclosed in a pressurized plenum. During a run, the stagnation temperature T_0 was held constant at 321 ± 2K, and the test section wall temperature remained close to ambient at T_w = 307 ± 3K. The tunnel wall boundary layers developed naturally and were fully turbulent upon arrival at the test section. Previous particle PIV measurements (unpublished) have indicated that the 99% wall boundary layer thickness at the cavity entrance is about 0.5 – 0.6 D for all flow conditions herein. The freestream Mach number M_∞ was varied from 0.55 – 0.90 and was measured with a static pressure tap in the tunnel sidewall at a position corresponding to the upstream edge of the cavity. The typical flow conditions for the experiments conducted in the 305 × 305 mm^2 test section are given in Table 1. The freestream dynamic pressure q_∞ was held constant for the majority of tests to a nominal value of about 33 kPa, since it is the appropriate scaling parameter for cavity pressures [3, 4].

Table 1: Typical TWT Experimental Conditions

M_∞	q_∞, kPa	Re × 10^{-6}, /m	L/W
0.55	33	18	1.00, 1.67, 5.00
0.80	33	13	1.00, 1.67, 5.00
0.90	33	13	1.67, 5.00

B. Cavity Geometries

The experiments used an insert that fit into the top wall of the test section. As shown in the left photo of Fig. 1, the insert contained a rectangular cavity cutout having a streamwise length L of 127 mm. The streamwise (x), wall-normal (y), spanwise (z) coordinate system originates at the spanwise center of the cavity leading edge. The wind tunnel ceiling is defined to be at $y = 0$. The floor of the cavity was formed from a piece of glass to provide a laser exit window. Similar to the previous supersonic study, experiments were run where the wall-normal cavity depth D was fixed at 25.4 mm and the spanwise width W was varied between 127 mm, 76.2 mm, and 25.4 mm to produce three different aspect ratios L/W of 1.00, 1.67, and 5.00. Additional details on the cavity hardware are given in [17]. As listed in Table 1, experiments were conducted at all three aspect ratios for $M_\infty = 0.55$ and 0.80. At $M_\infty = 0.90$, only the two narrower cavities were tested.

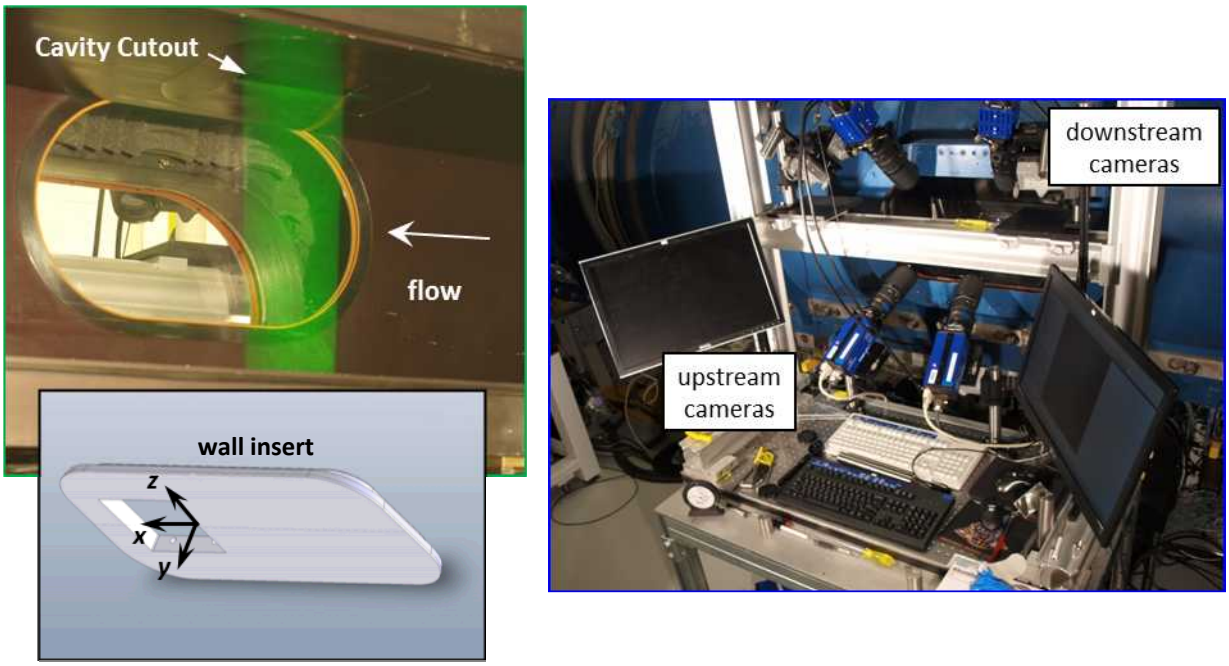

Fig. 1 TWT test section containing the cavity cutout and the PIV laser sheet that spanned the entire cavity length (upper left) along with the wall insert showing the coordinate system (lower left) and the stereoscopic PIV camera configuration used to simultaneously image the upstream and downstream portions of the cavity (right).

C. Cavity Pressure Measurements

A brief summary of the pressure measurements system is given here. Additional details can be found in [5]. Eight dynamic pressure sensors (Kulite XCQ-062-30A or similar) having a range of about 207 kPa and a flat frequency response up until about 50 kHz were placed in the cavity. The sensor locations are provided in Table 2. Four aft-wall sensors (AWP1-AWP4) recorded pressures over half of the cavity width. In addition, four fore-wall (FWP1-FWP4) sensors were used. The sampling frequency was 200 kHz and the data were low-pass-filtered at 50

Table 2: Fore-Wall Pressure (FWP), and Aft-Wall Pressure (AWP) sensor locations

Sensor #	*x/L*	*y/D*	*z/L*
FWP1	0.00	-0.50	0.00
FWP2	0.00	-0.50	-0.08
FWP3	0.00	-0.50	-0.20
FWP4	0.00	-0.50	-0.40
AWP1	1.00	-0.63	0.00
AWP2	1.00	-0.63	-0.08
AWP3	1.00	-0.63	-0.20
AWP4	1.00	-0.63	-0.40

kHz. Previous experiments have confirmed that the cavity pressures scale with q_∞, as expected [3, 4] and that the data are highly repeatable [5].

The frequency content of the pressure data is reported as *SPL* where the reference pressure is 20 μPa. In addition, coherence spectra between adjacent pressure sensors are given. All pressure spectra shown herein were generated using a total of at least 2 million samples and were computed using the Welch windowing algorithm in the Mathworks software package (MatLab R2013b). Blackman windows with an overlap of 50% were used. For the *SPL* spectra a window length of 10 Hz was chosen and for smoothing purposes, a longer window of 50 Hz was used for the coherence plots.

D. PIV measurements

Seeding was provided by a smoke generator (Corona Vi-Count 5000) that produced a large quantity of particles typically 0.2 - 0.3 μm in diameter from a mineral oil base. Particles were delivered to the tunnel stagnation chamber upstream of the flow conditioning section through a series of pipes and tubes, in which agglomeration of the particles occurred. Previous measurement of the *in-situ* particle response across a shock wave generated by a wedge showed the particle size to be 0.7 - 0.8 μm. Stokes numbers have been estimated as 0.04 [17] based on *a posteriori* measurements of typical cavity shear layer eddies, which is sufficiently small to rapidly attain the local velocity in the presence of velocity gradients in the shear layer [18, 19]. Inspection of PIV images of the recirculation region in the cavity showed that although the particle density drops, sufficient particles are retained for high vector quality in all regions.

The light source was a frequency-doubled dual-cavity Nd:YAG laser (Spectra Physics PIV-400) that produced about 300 mJ per beam. The beams were formed into coplanar sheets and directed into the test section from beneath the wind tunnel and then entered the cavity through the window forming its floor. The laser sheet thickness was about 1.0 mm, and as is shown in Fig. 1a, it was aligned to the spanwise center of the cavity and filled the entire streamwise length of the cavity. The time between laser pulses was varied between 1 and 2 μs depending on Mach number to produce streamwise displacements of about 15 pixels in the freestream.

As detailed in Beresh et al. [17], PIV measurements for rectangular cavities in the TWT are particularly challenging owing to limited optical access and the presence of the pressurized plenum that surrounds the test section. Since the cavities are three-dimensional (i.e., they do not span the entire test section width), solid walls obstruct a direct view of a submerged cavity cutout. To overcome this, the cameras were angled to view into the cavity depth. As shown in Fig. 1b, scattered laser light was collected by two sets of cameras. The first set imaged an upstream portion of the cavity ($0.25 < x/D < 2.20$) and the second set imaged a downstream portion ($1.7 < x/D < 4.7$). This four-camera configuration allowed for nearly the entire cavity to be imaged simultaneously and stereoscopically, without sacrificing spatial resolution.

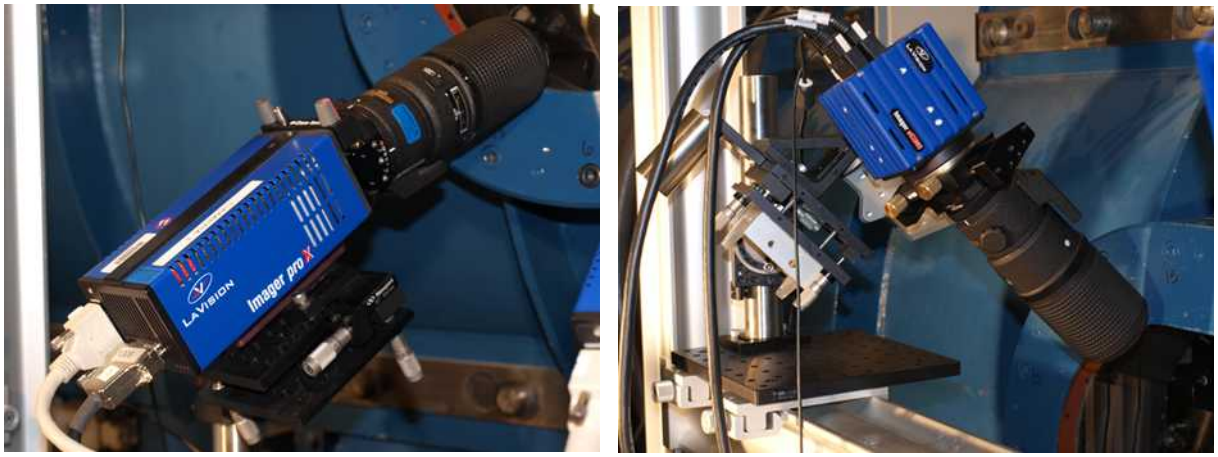

a) **b)**

Fig. 2 Cameras used in the dual-stereoscopic PIV system: a) an upstream-viewing camera, angled upward at an angle of about 40-degrees to view the ceiling-mounted cavity cutout, and b) a downstream-viewing camera, angled downward at an angle of about 55-degrees to view the cavity through the mirror mounted in the plenum.

The upstream stereoscopic imaging setup consisted of two interline-transfer CCD cameras (LaVision Imager ProX 4MP) with a resolution of 2048 × 2048 pixels digitized at 14 bits. The cameras were equipped with 200-mm lenses mounted on Scheimpflug platforms to create an oblique focal plane aligned with the laser sheet. Two-axis scheimpflug focusing was required for this configuration, which first was discussed by Walker [20] and subsequently has become standard in tomographic PIV [21]. The cameras viewed the imaging region using compound angles, where the half-angle with respect to the z direction was about 12-degrees. This 12-degree half-angle is sub-optimal for stereoscopic measurements; however, a greater angle would have resulted in increased occlusion of the field of view at the leading edge of the cavity. As shown in Fig. 2a, the upstream-view cameras were angled in the vertical plane at about 40-degrees to look into the cavity mounted in the ceiling. As a result, the entire D was viewed for the $L/W = 1.00$ geometry, whereas 0.70 D, and 0.25 D were viewable for the L/W and 1.67, and 5.00 geometries, respectively. A large f-number of 16 was chosen to increase the depth-of-field.

The downstream setup consisted of two sCMOS cameras (LaVision Imager sCMOS) with a resolution of 2560 × 2160 pixels digitized at 16 bits. The half-angle with respect to the z axis was also 12-degrees. Similar to the method used in [17], a mirror was mounted rigidly inside the plenum near the bottom wall to increase the vertical angle. As shown in Fig. 1b, the downstream cameras were angled downward at about 55-degrees to image the mirror. As a result of this steep angle, the entire cavity was visualized for the $L/W = 1.00$ and 1.67 geometries and for the narrowest cavity, about 50% of the depth was viewed. An f-number of 16 was also used for the downstream cameras lenses, which also had 200-mm focal length lenses fitted with scheimpflug platforms.

Stereoscopic camera calibrations were achieved by placing a single-plane alignment target in the position of the laser sheet, then scanning it through the volume of the laser sheet to acquire data at seven spanwise planes. The LaVision PIV software package DaVis v8.1 was used to find a polynomial fit for the calibration. The self-calibration routine in the software was also employed to reduce errors associated with misalignment between calibration target and the true location of the laser sheet.

At least 1000 realizations were used for each vector field shown herein. Image pairs were interrogated with an initial pass using 64 × 64 pixel interrogation windows, followed by two iterations of 32 × 32 pixel interrogation windows, incorporating adaptive window offsets and image deformation based upon local velocity gradients. A 50% overlap in the interrogation windows was used. The resulting vector fields were validated based upon signal-to-noise ratio, nearest-neighbor comparisons, and allowable velocity range. About 95% of all vectors obtained were valid and invalid vectors were filled with linear interpolation.

The interrogation window sizes of the upstream and downstream cameras were 0.38, and 0.45 mm, respectively. The two fields-of-view were combined to a single field for presentation purposes. This was accomplished by first removing edge-vectors from each field in the overlapping region ($1.7 < x/L < 2.2$). The views were then combined through linear interpolation to a single grid having a resolution of about 0.42 mm, using the software package Tecplot Focus 2013R1.

III. Results and Discussion

A. Effect of L/W on Mean Flow

Contours of mean streamwise velocity U are shown in Figures 3 – 5. Additionally, streamlines are superposed to visualize the recirculation region. For reference purposes, the contour scale is the same for each figure. For the two narrower cavities, the part of the flow occluded from the upstream cameras is masked with the white rectangle in the lower left hand corner. As previously mentioned, only about 0.5 D was visible in the downstream portion of the cavity at $L/W = 5.00$. Nevertheless, enough of the flow was captured to make useful observations. The white rectangles at the aft-end of the $L/W = 5.00$ cavity correspond to masked areas corrupted by large laser background levels, which could not be corrected. The background reflections for the narrowest cavity were the highest owing to the closer proximity of the cavity walls to the laser sheet. Similar masks are employed for the $L/W = 5.00$ data at the other two Mach numbers.

The Mach 0.55 data in Fig. 3 show that at $L/W = 1.00$, the shear layer protrudes into the freestream slightly more than the other two aspect ratios, although this difference is marginal. Notable differences do, however, exist in the recirculation regions. For instance, as the aspect ratio is increased from 1.00 to 1.67, the center of the recirculation moves upstream by about 0.1 D downward by about 0.2 D. As the cavity narrows to an aspect ratio of 5.00, the recirculation moves downstream significantly with its center at about $x/D = 4$. Murray et al. [4] made PIV measurements in a subsonic cavity having an $L/D = 6$ and an L/W of about 1. In their case, the cavity spanned the entire wind tunnel width and so three-dimensional effects are expected to differ from the present work where the flow is unconfined around the cavity. Nonetheless, at a similar Mach number, the recirculation region in [4] was close to the center of the cavity, which is similar to the $L/W = 1.00$ flow here.

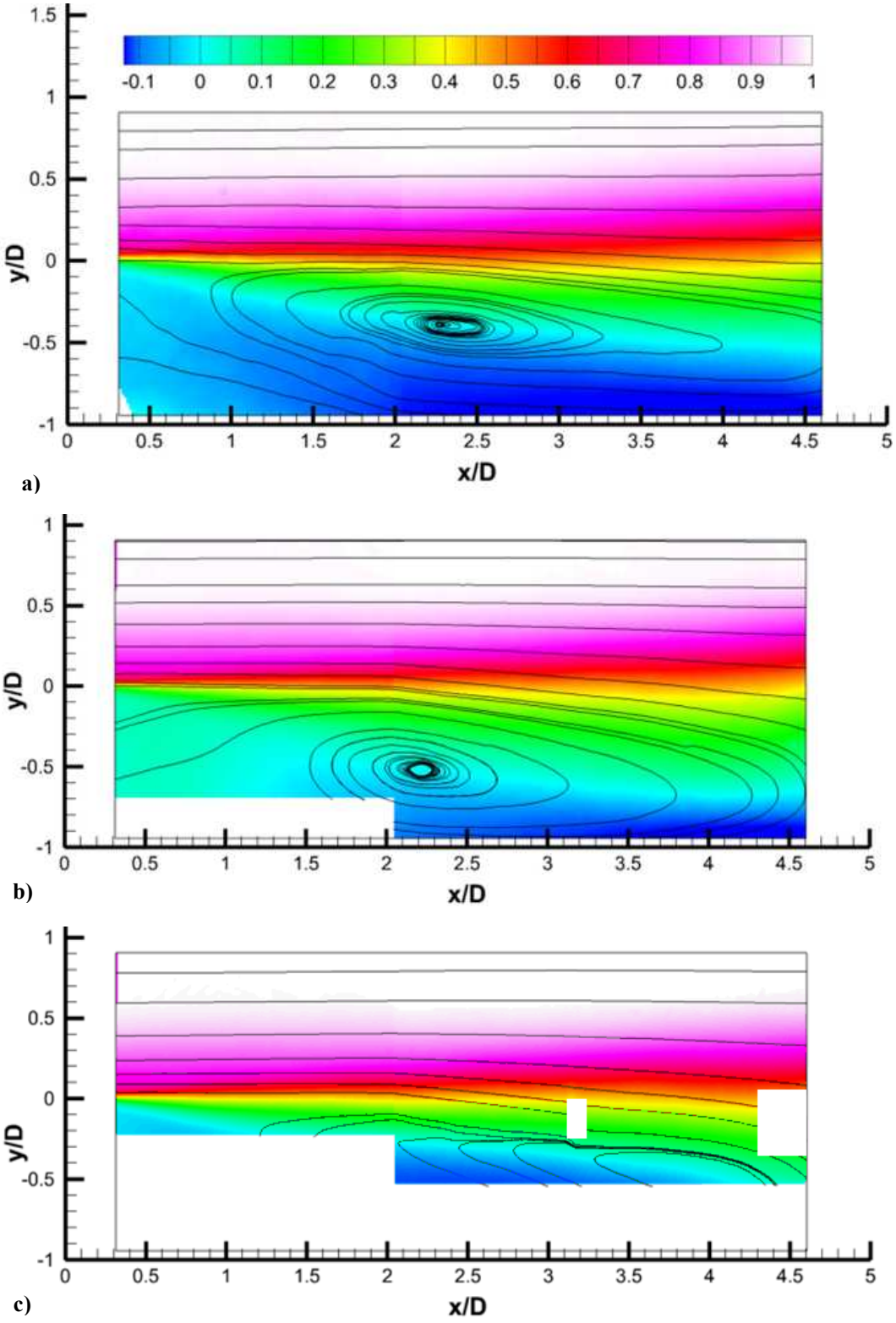

Fig. 3 Mach 0.55 mean streamwise velocity *U* contours with streamlines superposed at *L*/*W*: a) 1.00, b) 1.67, and c) 5.00. The recirculation region moves downstream at the highest *L*/*W*.

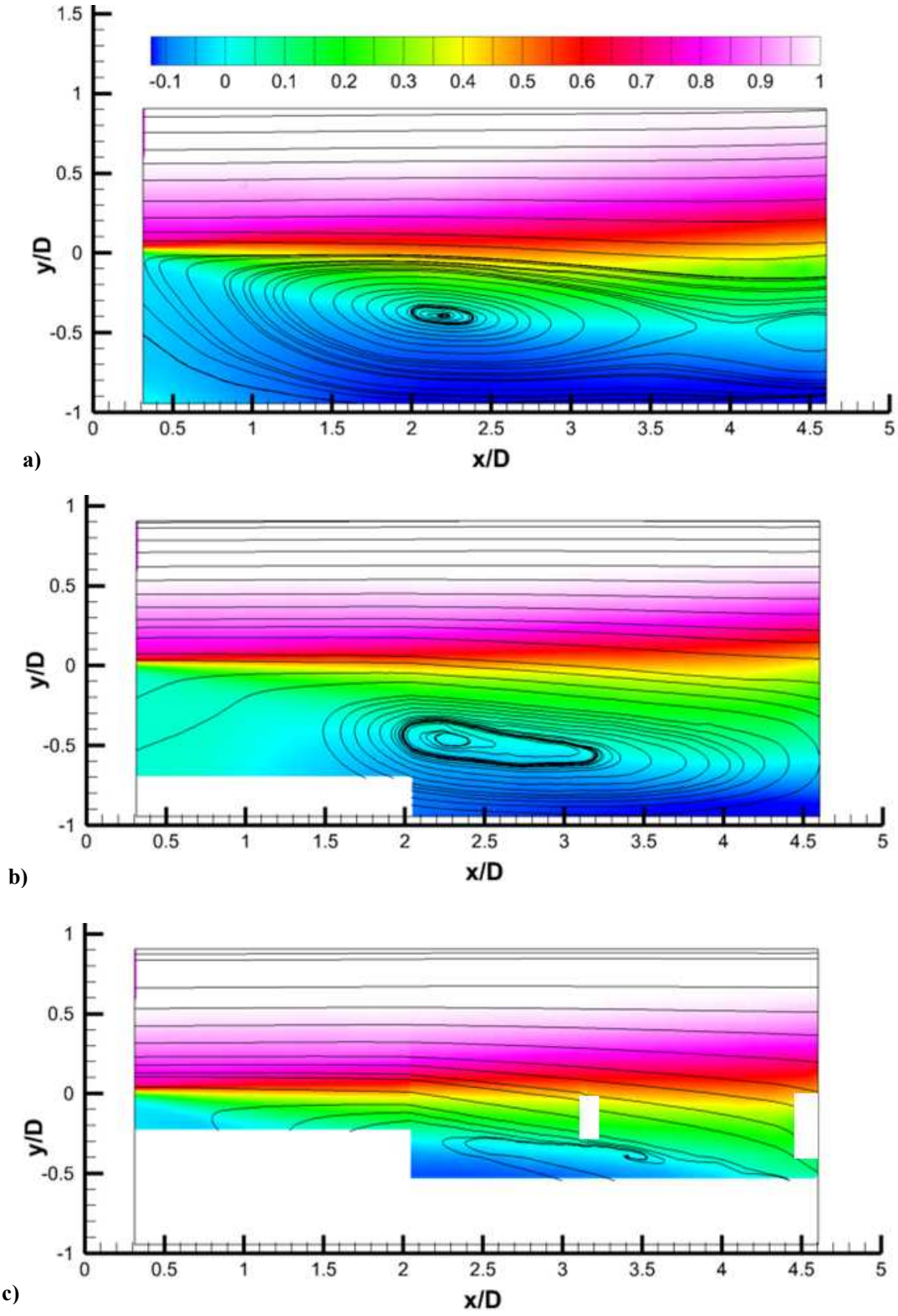

Fig. 4 Mach 0.80 mean streamwise velocity *U* contours and streamlines at *L*/*W*: a) 1.00, b) 1.67, and c) 5.00. The recirculation region moves downstream with increasing *L*/*W*.

U contours and streamlines are shown for the M_∞ = 0.80 cavity flows in Fig. 4. With L/W = 1.00, a primary recirculation region is observed near the cavity center, and a smaller, secondary recirculation region is observed at x/L = 4.5. Murray et al. [4] also reported similar flows with two circulation regions, although for lower Mach numbers near 0.4 and 0.6. Similar to M_∞ = 0.55, the primary recirculation moves downward by about 0.1 D when the cavity narrows from a square aspect ratio to L/W = 1.67. Also, similar to Mach 0.55, the recirculation region is centered for the two lower aspect ratios, but moves downstream at L/W = 5.00. In comparison to the Mach 0.55 data, at an L/W= 1.00, the recirculation region moves upstream slightly. Murray et al. [4] also reported an upstream movement of the recirculation region with increasing Mach number for their square aspect ratio cavity.

Mean flow data at Mach 0.90 are shown for L/W = 1.67 and 5.00 in Fig. 5. The data at L/W = 1.67 are quite similar to those at the other two Mach numbers, with a recirculation region close to the cavity center. Additionally, like the other two Mach numbers, the recirculation moves downstream at L/W = 5.00, although to a much lesser extent.

Finally, inspection of the mean flow data at each Mach number indicates that the L/W = 1.00 cavities tend to contain a stronger recirculation region than the L/W = 1.67 cavities. Furthermore, although the views for the L/W = 5.00 cavities are limited, it appears that the recirculation regions are also stronger than those at the middle aspect ratio, as evidenced by higher reverse flow velocities at an equivalent y location. This observation that the weakest recirculation region occurs in the L/W = 1.67 case is consistent with that observed in the supersonic experiments [17].

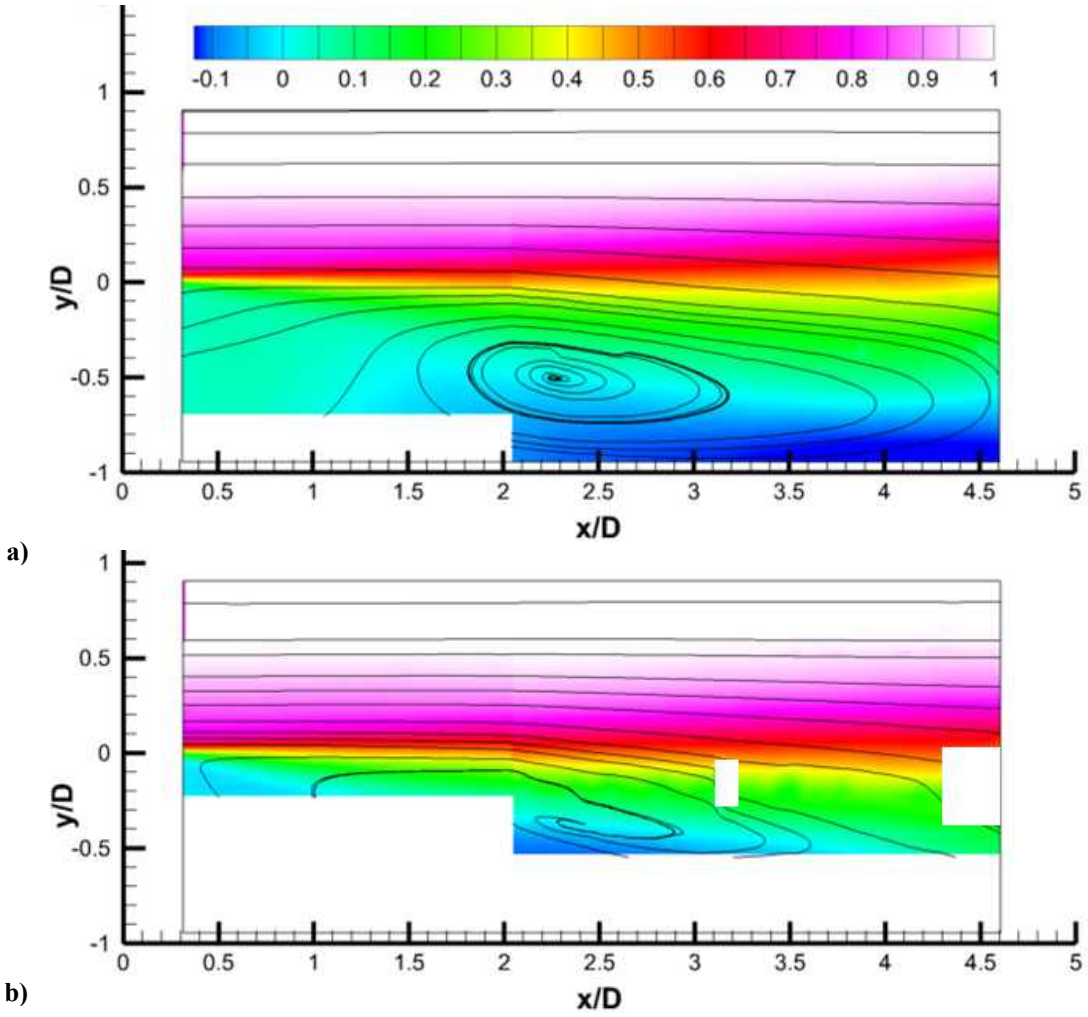

Fig. 5 Mach 0.90 mean streamwise velocity U contours and streamlines at L/W: a) 1.67, and b) 5.00. The recirculation region moves downstream only slightly at the highest L/W.

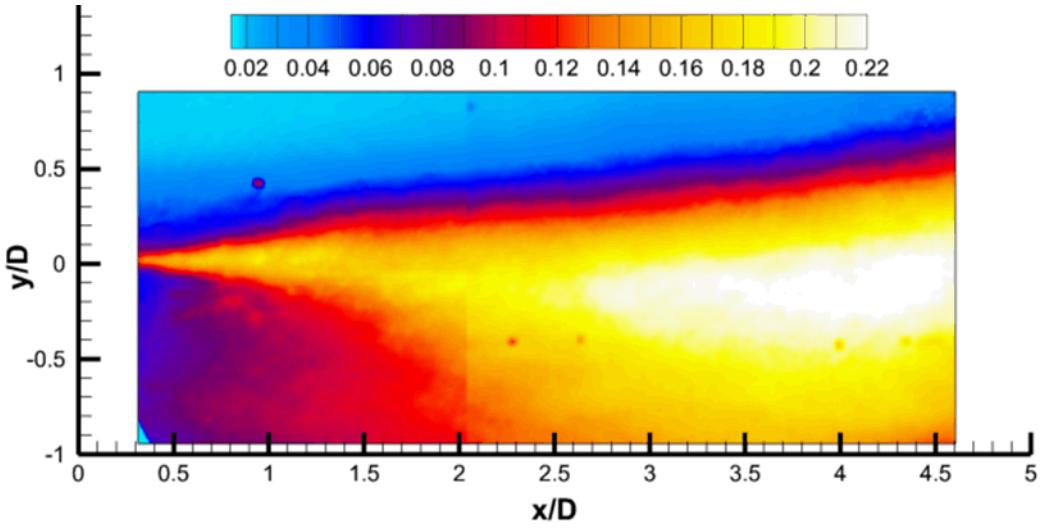

a)

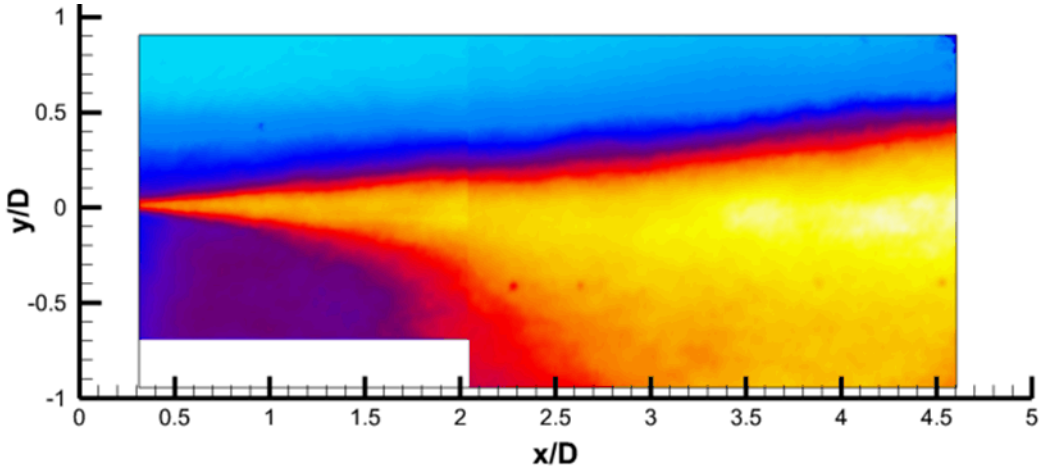

b)

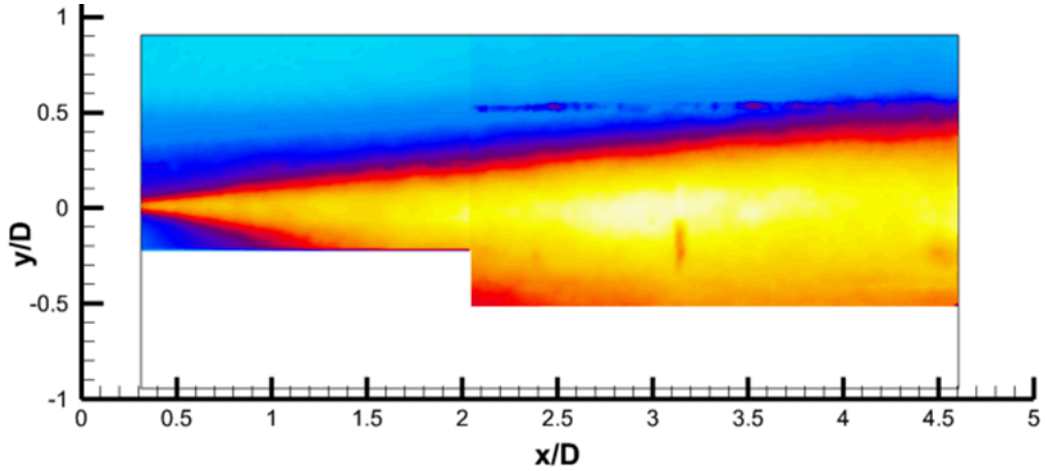

c)

B.

Fig. 6 Mach 0.55 streamwise turbulence intensity contours at *L*/*W*: a) 1.00, b) 1.67, and c) 5.00. The data show the turbulence levels to be diminished for the two higher L/W cases.

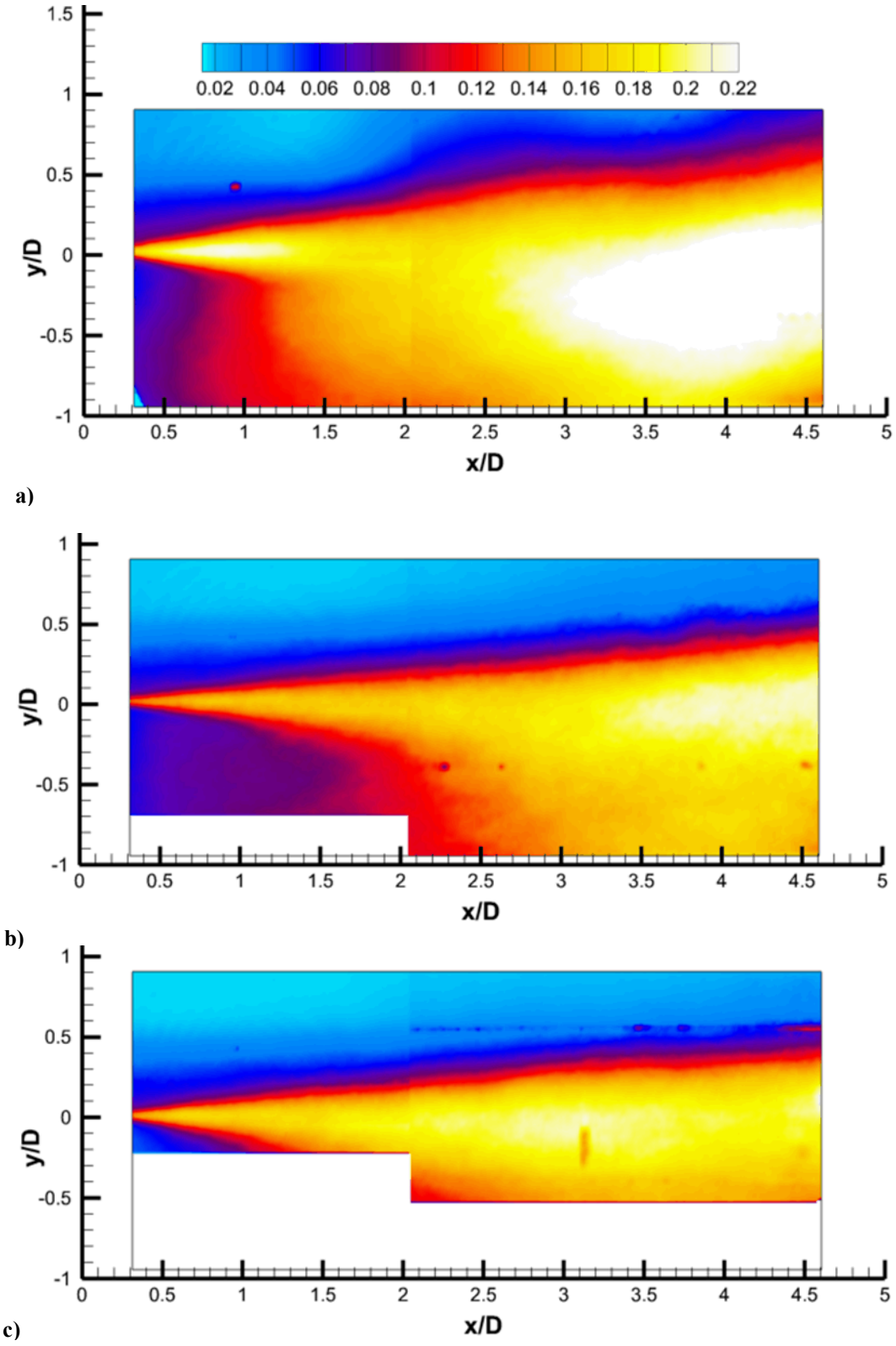

Fig. 7 Mach 0.80 streamwise turbulence intensity contours at *L*/*W*: a) 1.00, b) 1.67, and c) 5.00. The data show the turbulence levels to be diminished for the two higher L/W cases.

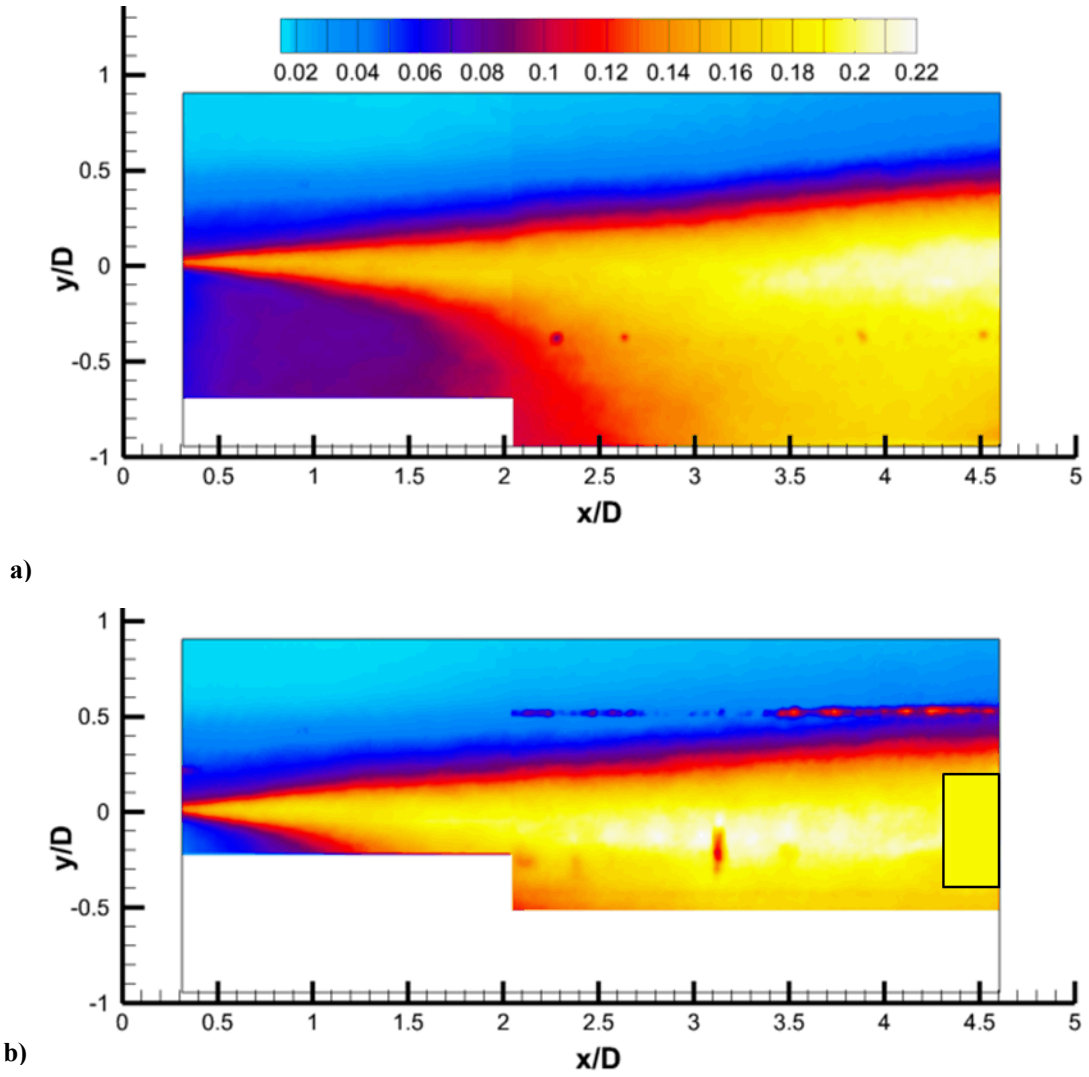

Fig. 8 Mach 0.90 streamwise turbulence intensity contours at L/W: a) 1.67, and b) 5.00. Comparisons between the geometries common to all three Mach numbers shows similar turbulence levels and distributions.

B. Effect of L/W on Turbulence Levels

Figures 6 – 8 present streamwise turbulence intensity contours at each Mach number, where the intensities have been normalized by U_∞ and each contour scale is again the same for comparison purposes. Over the range of geometries and Mach numbers, the peak turbulence intensity ranges from about 0.20 – 0.25, which is consistent with Ukeiley and Murray [16], who reported a range of 0.22 – 0.25 for an $L/W = 5$ cavity in a Mach 0.2 flow.

As shown in Fig. 6, at $M_\infty = 0.55$, the widest cavity exhibits the highest turbulence intensity, with a value of about 0.23. As the aspect ratio is increased, the turbulence levels decrease. For both the narrower cavities, the peak turbulence intensity is about 0.21. The distribution of turbulence is, however, different for the two narrower cavities. For instance, the peak intensity occurs near the aft-wall for the $L/W = 1.67$ geometry, but near $x/L = 3$ for $L/W = 5.00$.

The data in Fig. 7 corresponding to Mach 0.80 exhibit similar trends. The most turbulent case occurs in the square cavity, although at this Mach number, the peak intensity if about 0.25, compared to about 0.23 for Mach 0.55. In comparison to the square cavity, the two rectangular cavities once again have lower turbulence intensities, with peaks of about 0.20. Moreover, the distribution of turbulence within the cavity is similar to that at Mach 0.55.

The turbulence data for Mach 0.90 are shown in Fig. 8. The aft-end of the $L/W = 5.00$ plot is masked with a

yellow rectangle to cover the region corrupted by high levels of laser scattering. The data for both aspect ratios are quite similar to their counterparts at M_∞ = 0.55 and 0.80. For example, at a given L/W, the peak turbulence levels and the location of peak turbulence is observed to be consistent between Mach numbers.

Finally, the trend of the two narrower cavities showing diminished turbulence levels compared to the widest cavity is different from that observed in the supersonic experiments, where the L/W = 1.67 cavity was found to have the lowest turbulence in the streamwise – wall-normal symmetry plane [17].

C. Comparison of Turbulence and Pressure Fluctuations Levels

The peak turbulence intensity from each of the plots in Figures 6 – 8 is plotted as a function of pressure fluctuations measured with the aft-wall centerline sensor (AWP1) in Fig. 9. The data demonstrate a decreasing aspect ratio to be associated with lower turbulence intensities and pressure fluctuations.

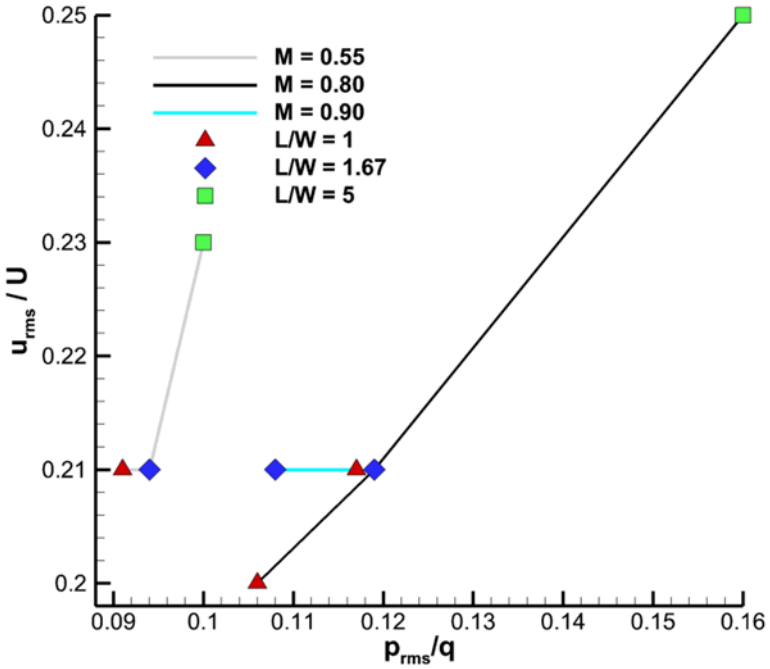

Fig. 9 Comparison of aft-wall centerline pressure fluctuations to turbulence intensity levels for each flow / configuration tested.

D. Cavity Pressure Spectra

The coherence between a sensor at the aft-wall centerline (AWP1) and a sensor offset in z by 0.4 D (AWP2) was computed and compared to the coherence between two fore-wall sensors (FWP1 and FWP2) offset by the same spanwise distance for each flow/configuration tested. The results are shown in Fig. 10, for the L/W = 1.67 cavity at Mach 0.55 and 0.89. The peaks in coherence below 4 kHz correspond to cavity resonant tones and are discussed subsequently with accompanying *SPL* plots. In both instances the flow coherence is greater at the fore-wall than that at the aft-wall. Similar observations were made for every geometry and flow tested. This is consistent with Zhuang et al. [22] who showed a greater fore-wall coherence for an L/D = 5, Mach 2 cavity flow, and hypothesized the greater upstream coherence to be related to disturbances that were primarily acoustic. They suggested the decreased coherence at the aft-wall to be caused by increased turbulence levels, which is clearly observed here in each contour plot of Figs. 6 – 8.

Fore-wall coherence levels at each L/W are compared at M_∞ = 0.55 in Fig. 11a. A similar comparison of aft-wall coherence is shown in Fig. 11b. At both the fore-wall and the aft-wall the spanwise coherence is greater for the narrowest cavity. Similar observations were made at each Mach 0.80 and 0.90. The higher coherence for the L/W = 5.00 cavity may be related to flow three-dimensionality. For example, in the supersonic experiments, PIV data

acquired in the $x - z$ plane just above the cavity showed the narrowest geometry to have the least amount of lateral (spanwise) flow. This result reproduced from [23] is shown in Fig. 12.

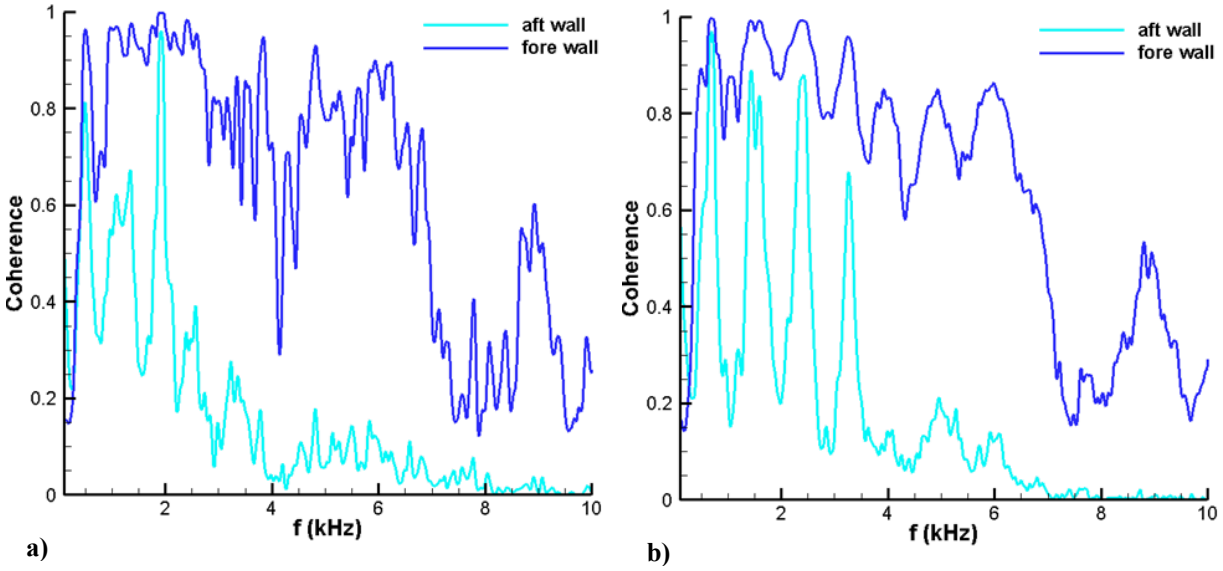

Fig. 10 Comparison of aft-wall and fore-wall coherence for the L/W = 1.67 cavity: a) Mach 0.55, and b) Mach 080. For all experiments, the fore-wall coherence was greater than the aft-wall.

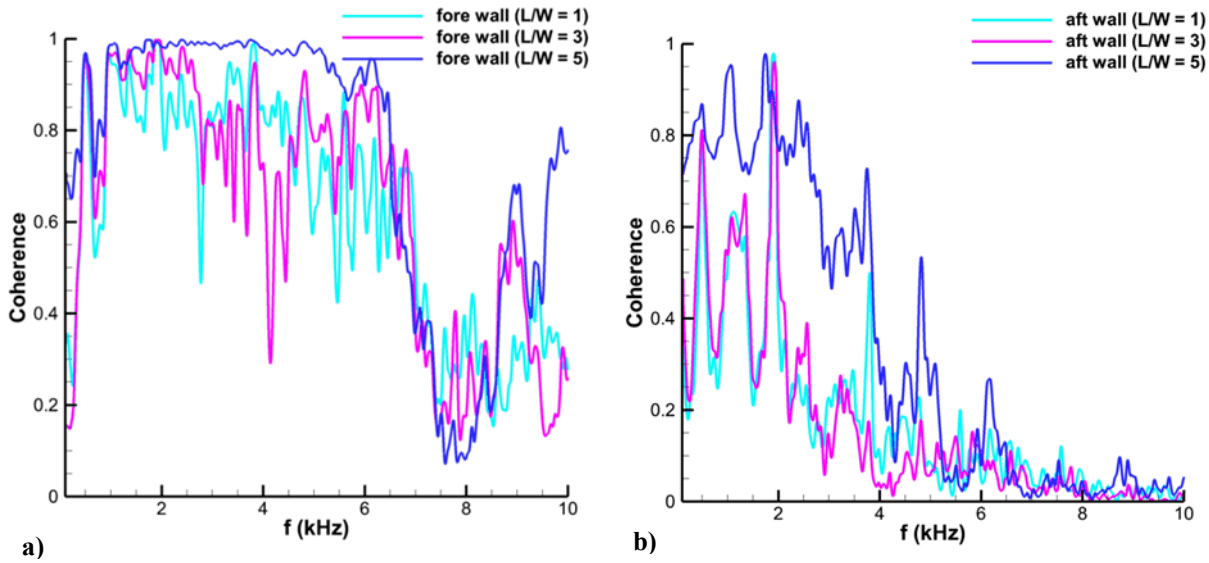

Fig. 11 Comparison of coherence for all three *L*/*W* at Mach 0.55: a) fore-wall, and b) aft-wall. For all Mach numbers tested, the *L*/*W* = 5.00 exhibited the greatest coherence.

The aft-wall centerline *SPL* spectra are shown for each Mach number and geometry in Fig. 13. The vertical lines, labeled R in Fig.13, show the cavity tone frequencies predicted by the modified Rossiter relation in [11], where the phase delay α and convective velocity ratio κ constants were set to the commonly used [24] values of 0.25 and 0.57, respectively. The theoretical cavity tone frequencies are seen to be in good agreement with those measured here.

The Mach 0.55 data (Fig. 13a) show that mode one occurs with small amplitude for each aspect ratio, and that mode 2 has significant energy in the narrowest cavity. Most significantly, cavity mode 3 is dominant regardless of *L*/*W*.

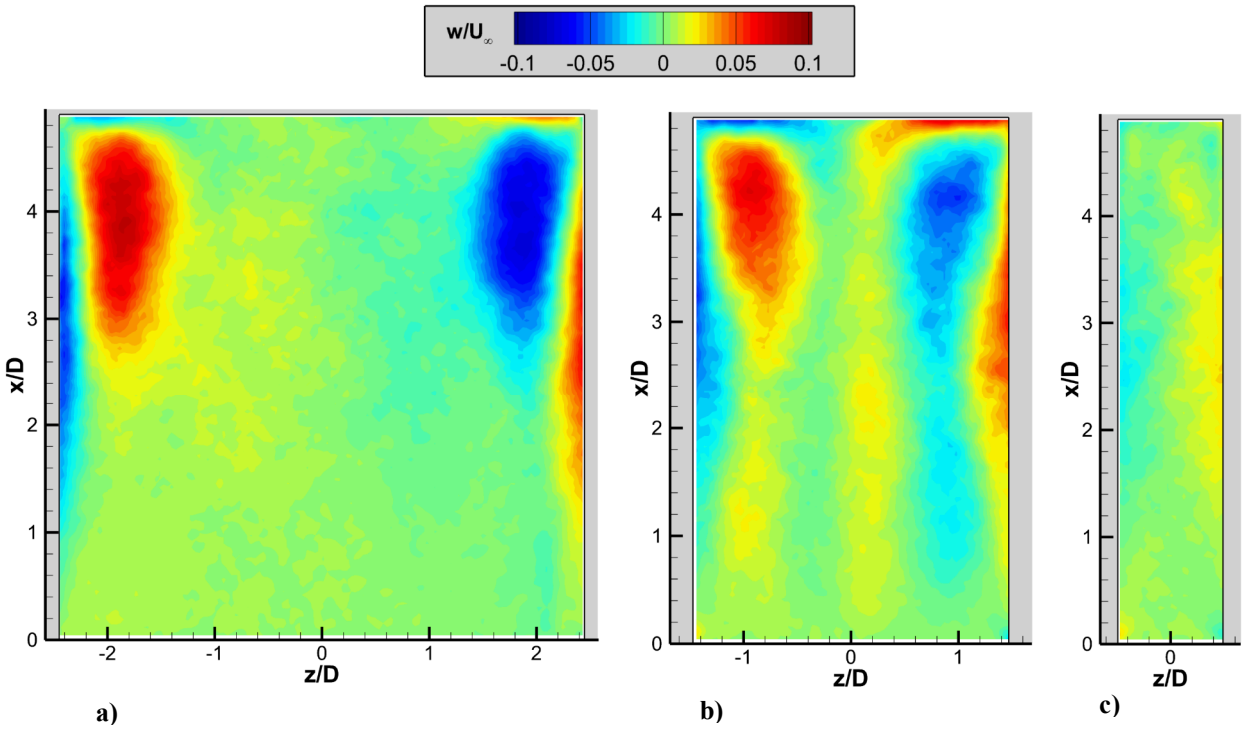

Fig. 12 Mach 2 comparison of mean spanwise velocity *w* just above the cavity (y/*D* = 0.05) with *L*/*W*: a) 1.00, b) 1.67, and c) 5.00. The figure reproduced from [23] indicates that the least spanwise flow occurs at *L*/*W* = 5.00.

In contrast, at Mach 0.8 (Fig. 13b), the *SPL* spectra are substantially different for each *L*/*W*. At *L*/*W* = 5.00, mode 2 is dominant and mode 3 also has significant energy. As the cavity widens to *L*/*W* = 1.67, mode 1 becomes dominant and peaks are seen at modes 2 – 4, with the amplitude decreasing with mode number. The spectrum at *L*/*W* = 1.00 exhibits a dominant mode 2, which is quite different from the other two aspect ratios at this Mach number.

The *SPL* spectra at Mach 0.90 (Fig. 13c) are fairly similar to those at Mach 0.80. As *L*/*W* widens, the dominant tone shifts from mode 2 to mode 1.

Overall, regardless of Mach number, modes 2 and 3 tend to be greatest for the *L*/*W* = 5.00 cavity. Trends for the other geometries, however, are not as obvious. For instance, in the *L*/*W* = 1.67 flows, the spectra do not resemble one another, unlike the mean and turbulence flow fields, which were quite similar for each Mach number. These observations suggest that additional research is required to understand better the mechanisms driving the dominant cavity mode selection.

IV. Conclusions

Experiments were conducted in subsonic and transonic open cavities having an *L*/*D* of 5. Three aspect ratios of 1.00, 1.67, and 5.00 were tested at three freestream Mach numbers of 0.55, 0.80, and 0.90. In all cases, the boundary layer at the cavity entrance was turbulent with a thickness of about 50 – 60% the cavity depth. The data complemented previous supersonic experiments conducted for the same cavity geometries at Mach numbers ranging from 1.5 – 2.5.

Two stereo PIV systems were used simultaneously, to visualize most of the cavity length along the streamwise symmetry plane. Mean velocity data showed the recirculation region to be centered in the cavity for the two wider geometries, whereas the recirculation region shifted downstream for narrowest cavity. At all Mach numbers, the recirculation region was weakest in the *L*/*W* = 1.67 cavity, a trend previously observed at the supersonic Mach numbers.

The *L*/*W* = 1.00 cavity had the highest streamwise intensities and aft-wall pressure fluctuations. The two narrower cavities exhibited lower turbulence intensities of a comparable level along with lower *OASPL*. In general,

the turbulence fields in the two narrower cavities were quite similar. This in contrast to the previous supersonic data, which showed minimum turbulence levels to occur for the $L/W = 1.67$ cavity.

At each Mach number, the narrowest cavity exhibited the greatest spanwise coherence at the fore and aft walls. This observation is possibly related to reduced spanwise flow in comparison to the wider cavities, which has been observed at Mach 2.

Cavity *SPL* spectra showed the narrowest cavity to have modes two and three active at all Mach numbers. However, despite very similar mean and turbulence flow fields for the $L/W = 1.67$ flows at each Mach number, the cavity *SPL* spectra were quite different. This observation highlights the need for new research into understanding what drives changes in mode shapes with cavity geometry, particularly, aspect ratio.

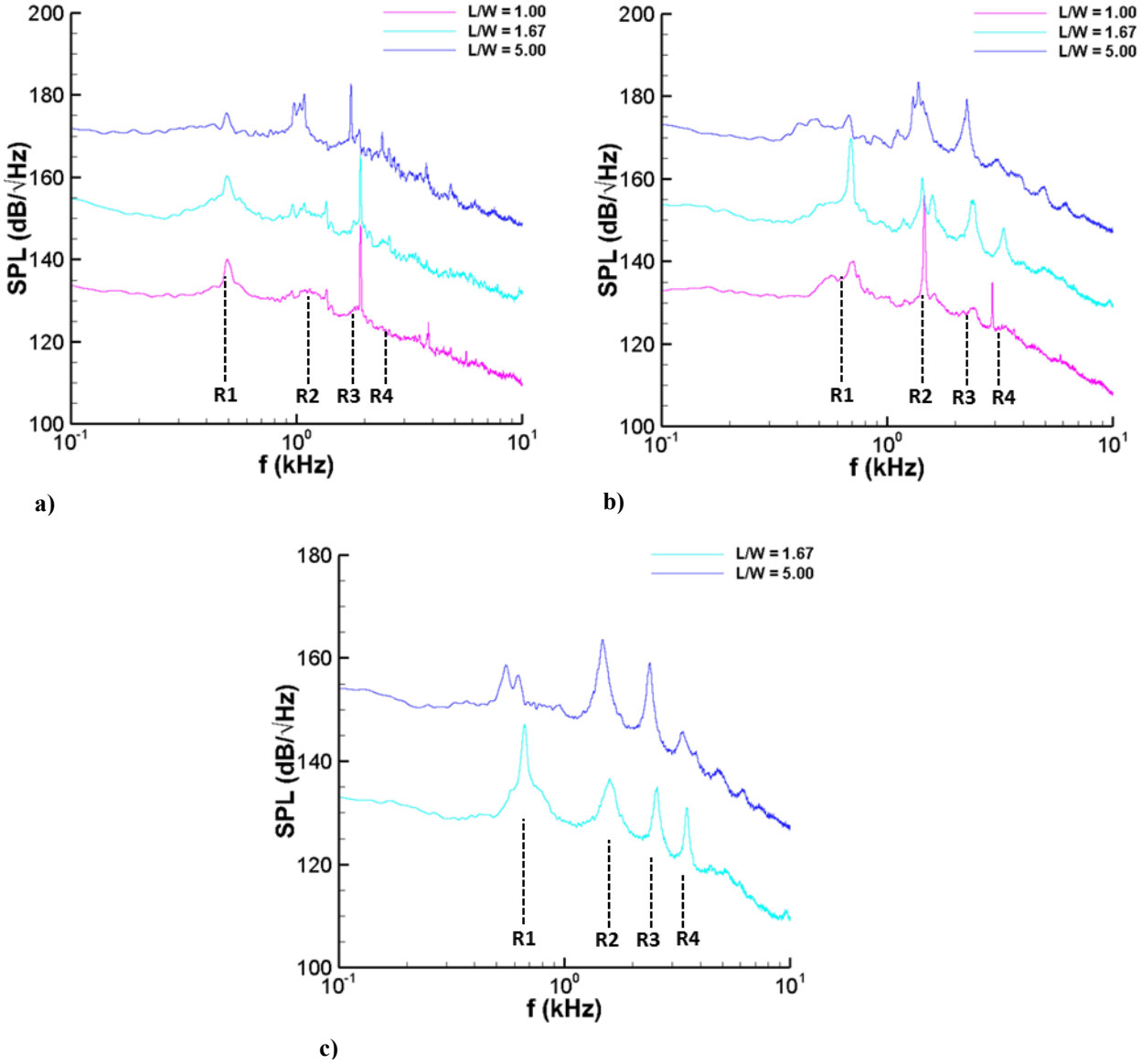

Fig. 13 Comparison of *SPL* with varying *L*/*W*: a) $M_\infty = 0.55$, b) $M_\infty = 0.80$, and c) $M_\infty = 0.90$. The spectra are offset by 20 dB for display purposes. The predicted [11] Rossiter tone frequencies (labeled R) are shown with dashed lines and are close to each of the measured tone frequencies.

Acknowledgments

The authors thank Srini Arunajatesen and Matthew Barone for helpful discussions on cavity flow physics and Bart Smith of Utah State University for tips on processing the PIV data.

References

[1]Rossiter, J. E., "Wind-Tunnel Experiments on the Flow Over Rectangular Cavities at Subsonic and Transonic Speeds," Aeronautical Research Council Reports and Memoranda, October 1964.

[2]Dix, R. E., and Bauer, R. C., "Experimental and Predicted Acoustic Amplitudes in a Rectangular Cavity," AIAA Paper 2000-0472.

[3]Tracy, M. B., and Plentovich, E. B., "Cavity Unsteady-Pressure Measurements at Subsonic and Transonic Speeds," NASA Technical Paper 3669, December 1997.

[4]Murray, N. E., Sallstrom, E., and Ukeiley, L., "Properties of Subsonic Open Cavity Flow Fields," *Physics of Fluids*, Vol. 21, No. 9, 2009.

[5]Wagner, J. L., Casper, K. M., Beresh, S. J., Hunter, P. S., Spillers, R. W., Henfling, J. F., Mayes, R. L., "Experimental Investigation of Fluid-Structure Interactions in Compressible Cavity Flows," AIAA Paper 2013-3172.

[6]Rockwell, D., and Naudascher, E., "Review-Self Sustaining Oscillations of Flow Past Cavities," *Journal of Fluids Engineering*, Vol. 100, 1978, pp. 152-165.

[7]Rowley, C. W., and Williams, D. R., "Dynamics and Control of High-Reynolds-Number Flow over Open Cavities," *Annual Review of Fluid Mechanics*, Vol. 38, 2006, pp. 251-276.

[8]Cattafesta et al. Review in *Progress in Aerospace Sciences*, 2008

[9]Unalmis and Clemens, AIAAJ 2001.

[10]Stallings, R. L., and Wilcox, F. J., "Experimental Cavity Pressure Distributions at Supersonic Speeds," NASA Technical Paper 2683, June 1987.

[11]Heller, H. H., and Bliss, D. B., "The Physical Mechanism of Flow Induced Pressure Fluctuations in Cavities and Concepts for Suppression," AIAA Paper 75-491.

[12]Kegerise, M. A., Spina, E. F., Garg, S., Cattafesta, L. N., "Mode-switching and nonlinear effects in compressible flow over a cavity," Physics of Fluids, Vol. 16, No. 3, 2005, pp. 678-687.

[13]Larcheveque et al. JFM 2004 (LES paper).

[14]Murray, N. E., and Ukeiley, L. S., "Modified quadratic stochastic estimation of resonating subsonic cavity flow," Journal of Turbulence, Vol. 8, No. 53, 2007, pp. 1-22.

[15]Flaherty, W., Reedy, M. T., Elliot, G. S., Austin, J. M., Schmit, Crafton, J., "Investigation of Cavity Flow Using Fast-Response Pressure Sensitive Paint," AIAA Paper 2013-0678.

[16]Ukeiley, L. S., and Murray, N. E., "Velocity and Surface Pressure Measurements in an Open Cavity," Experiments in Fluids, Vol. 38, 2005, pp. 656–671.

[17]Beresh, S. J., Wagner, J. L., Pruett, B. O., "Supersonic Flow over a Finite-Width Rectangular Cavity," AIAA Paper 2013-0389, Jan. 2013.

[18]Samimy, M., and Lele, S. K., "Motion of Particles with Inertia in a Compressible Free Shear Layer," Physics of Fluids A, Vol. 3, No. 8, 1991, pp. 1915-1923.

[19]Melling, A., "Tracer Particles and Seeding for Particle Image Velocimetry," Measurement Science and Technology, Vol. 8, No. 12, 1997, pp. 1406-1416.

[20]Walker, S., "Two-Axes Scheimpflug Focusing for Particle Image Velocimetry," Measurement Science and Technology, Vol. 13, No. 1, 2002, pp. 1-12.

[21]Elsinga, G. E., Scarano, F., Wieneke, B., and van Oudheusden, B. W., "Tomographic Particle Image Velocimetry," Experiments in Fluids, Vol. 41, No. 6, 2006, pp. 933-947.

[22]Zhuang, N., Alvi, F. S., Alkislar, M. B., and Shih, C., "Supersonic Cavity Flows and Their Control," *AIAA Journal*, Vol. 44, No. 9, 2006, pp. 2118-2128.

[23]Beresh, S. J., Wagner, J. L., Pruett, B. O., Henfling, J. H., and Spillers, R. W., "Supersonic Flow over a Finite-Width Rectangular Cavity," *submitted to AIAA Journal*, October 2013.

[24]Arunajatesen, S., Kannepalli, C., Sinha, N., Sheehan, M., Alvi, F., Shumway, G., and Ukeiley, L., "Suppression of Cavity Loads Using Leading-Edge Blowing," *AIAA Journal*, Vol. 47, No. 5, 2009, pp. 1132-1144.